LASER INTERFEROMETER GRAVITATIONAL WAVE OBSERVATORY
- LIGO -
CALIFORNIA INSTITUTE OF TECHNOLOGY
MASSACHUSETTS INSTITUTE OF TECHNOLOGY

Technical Note	**LIGO-T11XXXXX–vX**	2017/10/02

Temperature Control and Coupled Oscillator Modelling for LIGO Voyager

Jordan Kemp, Brittany Kamai, Aaron Markowitz

California Institute of Technology
LIGO Project, MS 18-34
Pasadena, CA 91125
Phone (626) 395-2129
Fax (626) 304-9834
E-mail: info@ligo.caltech.edu

Massachusetts Institute of Technology
LIGO Project, Room NW22-295
Cambridge, MA 02139
Phone (617) 253-4824
Fax (617) 253-7014
E-mail: info@ligo.mit.edu

LIGO Hanford Observatory
Route 10, Mile Marker 2
Richland, WA 99352
Phone (509) 372-8106
Fax (509) 372-8137
E-mail: info@ligo.caltech.edu

LIGO Livingston Observatory
19100 LIGO Lane
Livingston, LA 70754
Phone (225) 686-3100
Fax (225) 686-7189
E-mail: info@ligo.caltech.edu

http://www.ligo.caltech.edu/

Abstract

In 2022, the Laser Interferometer Gravitational-Wave Observatory (LIGO) project will undergo its transition from its third iteration, A+, to its fourth iteration, Voyager. LIGO Voyager intends to reduce coating thermal noise by operating LIGO at cryogenic temperatures and replacing fused silica optics with silicon. My summer research with the Voyager group addressed the cooling of the planned thermal shields surrounding the LIGO optics using copper straps, the parameter optimization of a ringdown experiment to determine the loss of optics coatings, and determining the temperature dependence of the eigenfrequencies of bulk silicon to develop a method of decoupled temperature determination. Our findings suggest that the F designated copper straps cool more efficiently than S and L straps with a thermal conductance constant of .06721±.0009W/K. We have produced an approximation of the error budget for the ringdown measurement which suggests that the uncertainty in the loss angle of the disk and coupled system most strongly influences the error in our loss measurement, and precise measurement of these parameters will result in the most precise results. We have also produced an apparatus for calibrating the temperature dependence of the eigenfrequencies of silicon disks.

1 Introduction and Objectives

On September 14, 2015, the Advanced Laser Interferometer Gravitational-Wave Observatory (LIGO), a second-generation detector, detected gravitational waves emanating from a binary black hole merger. While this was a milestone for the development of gravitational-wave astronomy, LIGO's capabilities are still limited in its most sensitive frequency band by, among other sources, Brownian thermal noise. LIGO Voyager is a working plan to upgrade LIGO to a fourth generation detector that pushes the precision limit of the current infrastructure by tackling the issue of Brownian thermal noise.

Geometric stability in the reflective optics used in the Fabry-Perot cavity arms of LIGO are paramount to limiting phase noise. In addition to inducing Brownian thermal noise by exciting the reflective particles on the test mass's surface, the 30kW laser introduces phase noise by causing the surface of the test mass to thermoelastically expand, changing the pathlength of the laser. Fortunately, silicon at a temperature of 123K has a coefficient of thermal expansion of zero, experiences less Brownian thermal noise than fused silica, and has a Q similar to that of fused silica, the material currently used in LIGO test masses. Therefore characterizing the thermal and mechanical properties of silicon and the candidate reflective and emissive coatings are important to the development of LIGO Voyager.

My summer research contributed to three main categories of Voyager development:

1. Determining the mechanical loss angle of the coatings
2. Tracking the temperature of the test silicon disks for cryogenic Q measurements
3. Cooling the test mass apparatus without mechanically coupling them to the environment.

1.1 Mechanical Loss of Coatings

The mechanical loss of a material's oscillation, such as a resonating laser cavity or vibrations on the surface of a material, is a measurement of the fraction of elastic energy

lost with each oscillation cycle. An object with a low mechanical loss, and similarly a high quality factor, has well defined vibrational modes in narrow frequency bands that retain much more energy after a given period of oscillation than a lossy, low quality material. For a measurement sensitive to fluctuations in an object's motion, such as the power spectrum of some mechanical system, system components with high quality factors is an attractive feature. They will allow much of the noise to be subtracted out of the data by applying band pass filters, as most of the absorbed noise will be localized to peaks whose location can be predicted by characterizing the system beforehand.

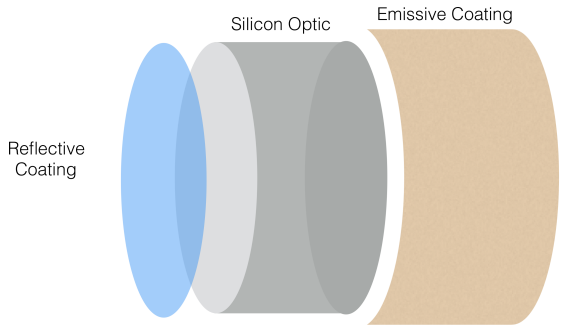

Figure 1: A diagram of the relations between the reflective and emissive coatings to be tested for the silicon optics. The primary reflective coating candidate, amorphous silicon, will be deposited on the front of the mirror. The emissive coating, used for the radiative cooling of the test mass, will be deposited on the barrel of the optic.

Therefore, when preparing a new test mass system consisting of a silicon bulk, amorphous silica reflective coating, and emissive barrel coating, characterizing the location and quality factor of each of the vibrational modes is an essential task for reducing noise. LIGO Voyage currently employs a method of determining these properties in bulk test mass materials called the Gentle Nodal Suspension, or GeNS.

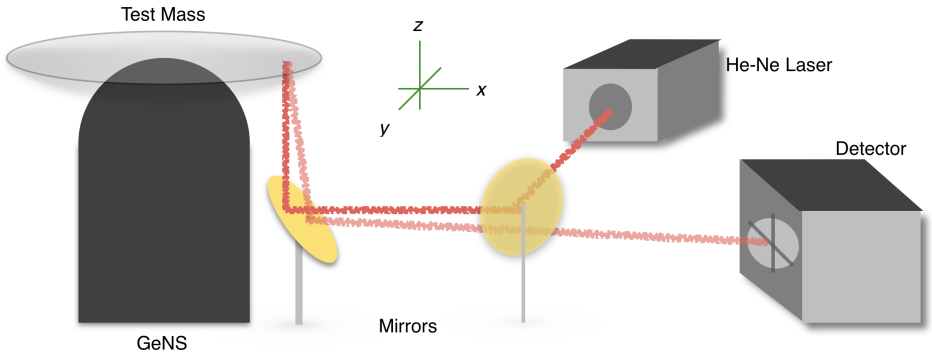

Figure 2: A diagram of the the GeNS setup used by LIGO Voyager. The silicon disk is centered on a hemisphere at a single point of contact so that there is minimal mechanical coupling between the disk and the mount. A laser is emitted , and reflected off of the underside of the disk into a quadrant photodetector (QPD). As the mechanical modes disk is excited (generally by an electrostatic drive), the vibrating disk shakes the beam that is reflected into the QPD. Performing a Fourier Transform on the time series signal produces the power spectrum of the disk's vibrations. By measuring the characteristic ringdown time from excited state to rest of any mode yields the mode's loss angle.

While GeNS is an ideal setup for an object for determing the loss in a good oscillator characteristics, such as a rigid disk, it is less effective in directly measuring the loss angle of an object with poor oscillator quialities, such as an amorphous coating. The GeNS, nonetheless, can still be useful for indirectly measuring the coating's loss angle. Consider the equation for loss angle of a system consisting of a single oscillator.

$$\phi_1 = \frac{1}{Q_1} \tag{1}$$

Where the loss angle, ϕ, is simply the reciprocal of that object's quality factor. For a system composed of two separate, yet mechanically coupled objects the mechanical loss of the system becomes a linear combination of the individual loss angles scaled by their relative elastic potential energy contribution to the system.

$$\phi_{system} = (1 - D)\phi_1 + D\phi_2 \tag{2}$$

Where ϕ_1 is the loss angle of a good oschillator, ϕ_2 is of poor oscillator, and D is the dilution factor, approximating the second oscillator as a solute deposited on the oscillator 1. This equation can be solved for either of the loss angles.

$$\phi_2 = \frac{1 - D}{D}\phi_1 + \frac{1}{D}\phi_{system} \tag{3}$$

With the equation in this form, it is possible to determine the loss angle of the second, poor oscillator. Given an oscillator 1 of known loss angle, a measurement of the system loss angle can be used as a parameter in determining the loss angle of the poor oscillator. Put simply, by measuring the quality factor of a sample silicon disk before and after depositing a known amount of the coating in question on the disk, the loss angle of the coating can be easily calculated.

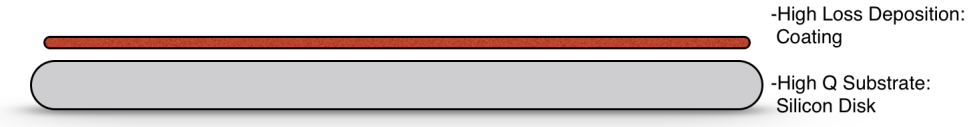

Figure 3: A diagram of the reflective coating deposited on the surface of the silicon disk

Before doing an experiment of this kind, it is important to optimize the experiment so that propagated errors from systematic uncertainties in the parameter measurements can be minimized. While this would normally be done using finite element analysis of the experiemental system with software such as COMSOL, such analyses are computationally expensive with results that are often difficult to analyze. Therefore, it is worthwhile to develop an intutition for how the parameters interact within the system by analyzing a more simplified model. Part of my SURF project involved creating and analyzing an analytical coupled harmonic oscillator model. By formulating the equations for error propagation of the parameters of the coupled harmonic oscillator, and analyzing them for values we expect to see in the lab, it is possible to determine which parameters are primary error contributors. With that information, we can create a heirarchy of variables in terms of importance in mitigating error in our ringdown measurement.

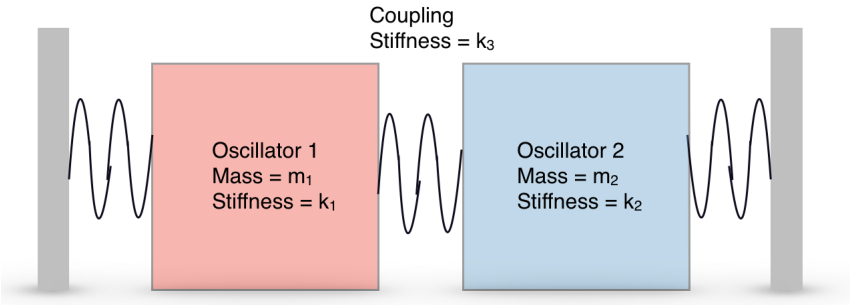

Figure 4: A diagram of the simplified harmonic oscillator model. The coating and bulk disk are reduced to masses coupled by some factor k_3. The objects elastic properties, such as Young's modulus, Poisson's ration, and bulk and shear modulus are stored in their respective k values. The oscillators also have characteristic loss angles, ϕ

.

1.2 Temperature Tracking of Cryogenic Silicon

The characterization of silicon's mechanical properties at cryogenic termperatures requires that the temperature of the disk be known during experimentation. Using conventional thermal contact probing methods mechanically couples the disk to its environment beyond what was intended with the GeNS system. Therefore, there is some motivation for developing a method for tracking the temperature that does not involve conduction through a contact.

As objects are cooled from room temperature, the intermolecular spacing decreases. This causes a number of phenomena to occur, such as bulk to become brittle or contract. Most relevant to our research, this temperature modulation causes shifts in the elastic characteristics of the bulk, such as the Young's modulus and Poisson's ration. Given the inherent relationship between the elastic and mechanical behaviors in oscillators, this temperature change translates to some shift in the location of the mechanical modes in frequency space. Thus, the calibrated location of the mechanical modes can be used as an indirect measurement of the temperature of the disk. My second SURF project this summer involved setting up a modified GeNS system that could calibrate the mechanical mode frequency dependence of silicon disks.

1.3 Thermal Conductance of Copper Straps

LIGO Voyager has developed plans for the cryogenic apparatus for the Voyager test masses. They will be encased in multiple layers of thermal shields, whose lower temperature will facilitate the test masses' emissive cooling during operation. Each thermal shield will be mechanically decoupled from the environment using a series of cantilever springs, similar to the test mass. The shields will be conductively cooled with the use of copper straps that link the shields to some heat sink. The low specific heat capacity and large surface area of the copper braids make them excellent for removing heat from a system. By damping any vibrations in the braids, we should be able to provide a quiet heat sink for the test masses. This setup will provide the test masses with a cold environment to which it can radiate heat onto, allowing the test masses to maintain a low temperature without the mechanical coupling induced by contact cooling.

To further Voyager planning, candidates for the copper straps must be identified, and their mechanical properties and cooling power must be characterized. The cooling power is particularly important, as it will determine how good of heat sink these straps

can be as they maintain LIGO's cryogenic temperature. Given a sample copper strap, this property can be experimentally determined.

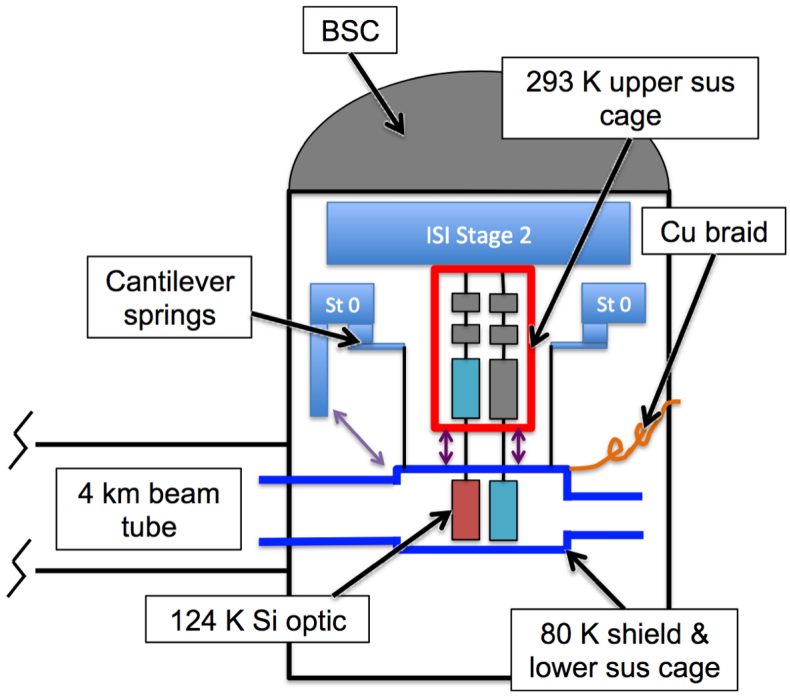

Figure 5: A simplified plan of the Voyager upgrades within one of the Fabry-Perot cavities. Multiple thermal shields will be set up in a stepwise fashion as to provide the test mass a cooler background for thermal emissions while mechanically decoupling the test mass from the environment and noisy components of the liquid nitrogen apparatus. The copper braids will sink heat from the shields into the liquid nitrogen supply.

The thermal conductance of a material relates the temperature gradient across the material, ΔT, to some amount of power dissipated P. The equation for thermal conductance is

$$P = k\Delta T \tag{4}$$

Therefore, the conductance is a quantity unique to an object, modelling it as a black-box heat transfering body. This method is useful for identifying copper strap candidates, as its independence of geometry and composite materials allows for direct comparion between different straps. The last SURF project I worked on involved determining this conductance value for different copper strap candidates.

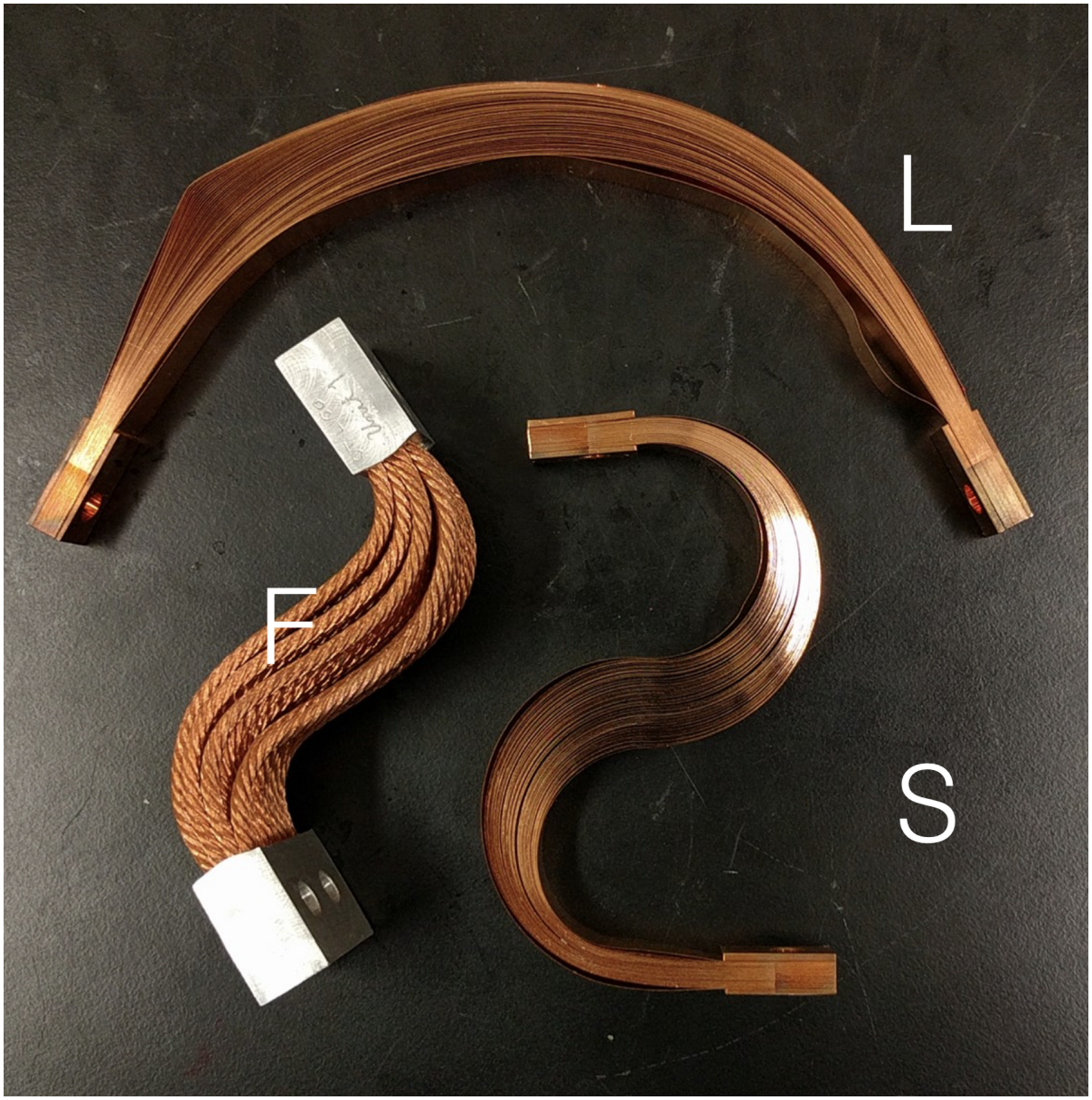

Figure 6: The three copper strap candidates include an L shaped strap consisting of 70 thin copper bands. The S shaped strap is of the same material as the L strap. The braided strap, denoted F, consists of copper braids.

2 Method and Results

2.1 Coatings Mechanical Losee: Coupled Harmonic Oscillator Model

The coupled harmonic oscillator system can be used as an approximation for the system consisting of a coating deposited on some substrate. Much like oscillators, the substrate and coating resonante at identity frequencies with quality factors and loss angles defined by their own internal composition.

Upon mechanically coupling the substrate and coating, much like when harmonic oscillators are coupled, the system will develop eigenfrequencies and ringdown behaviors unique to the system. Under this condition, the ringdown behavior of the individual

oscillators are now coupled as energy is exchanged back and forth between the oscillators. Therefore, in order to understand the ringdown behavior of a coupled system, we must build an intuition for the behavior of the individual oscillators when coupled.

2.1.1 Loss Angle of a Isolated Damped Oscillator

The mechanical spring constant of a harmonic oscillator, k, can be decomposed into a real component, with magnitude k_r, and an imaginary component, with magnitude k_i.

$$k = k_r + ik_i \tag{5}$$

The imaginary component can be derived from the general equation for k, and is expressed as the product of the real component, and the loss angle, ϕ.

$$k = k_r(1 + i\phi^2) \tag{6}$$

The loss angle can be solved for using equations 5 and 6,

$$\phi = \sqrt{\frac{k_i}{k_r}} \tag{7}$$

This loss angle quantifies the ringdown behavior of a damped harmonic oscillator, which assumes the following form

$$x(t) = e^{ik_r t - k_i t} \tag{8}$$

Where the real component expresses the oscillation, and the imaginary component expresses the oscillation's exponential decay. The equation displays the loss angle's directly proportionality to rate of decay of a particular frequency rings down with respect to time. For a completely uncoupled oscillator, the loss angle is the reciprocal of the quality factor, Q, a measure of the amount of oscillations required to dissipate energy at a specific frequency.

$$Q = \frac{1}{\phi} \tag{9}$$

2.1.2 Loss Angle of a Coupled Oscillator

The loss angle of mechanically coupled oscillators takes the form of a linear sum of the oscillators' individual loss angles, weighted by the mechanical energy of each individual oscillator.

$$\phi_{system} = \frac{E_1}{E_{system}}\phi_1 + \frac{E_2}{E_{system}}\phi_2 \tag{10}$$

Where mechanical energy is quantified by the average potential energy stored by the individual oscillators. In the case of the oscillators of Figure **??**, the mechanical energies are

$$E_1 = \frac{1}{2}\Big(k_1 x_1^2 + k_3(x_1 - x_2)^2\Big) \tag{11}$$

$$E_2 = \frac{1}{2}\Big(k_2 x_2^2 + k_3(x_2 - x_1)^2\Big) \tag{12}$$

$$E_{Total} = E_1 + E_2 - \frac{1}{2}k_3(x_1 - x_2)^2 \tag{13}$$

The coupling of the energies can be seen in the shared $k_3(x_1 - x_2)^2$ factor, which must be subtracted from equation 13 to eliminate redundancy. We can solve equation 10 for ϕ_2

$$\phi_2 = \frac{E_{system}}{E_2}\phi_{system} - \frac{E_1}{E_2}\phi_1 \tag{14}$$

This expression allows the loss angle of the second oscillator to be symbolically derived using a combination of the experimental ringdown of the coupled system, the known ringdown behavior of one of the first oscillator, and experimental parameters defining the energy within the system.

By substituting the definition of loss angle, 9, for Q_{system} and Q_1, as well as the definitions for energy expressed in equations 11 through 12, equation 14 can be expressed as

$$\phi_2 = \frac{1}{Q_{system}}\left(1 + \frac{k_1 x_1^2}{(k_2 x_2^2 + k_3(x_1 - x_2)^2)}\right) - \frac{1}{Q_1}\frac{k_1 x_1^2 + k_3(x_1 - x_2)^2}{k_2 x_2^2 + k_3(x_1 - x_2)^2)} \tag{15}$$

To reduce this equation to the parameters of the system (ie, masses and spring constants), we must solve the equations of motion. This will provide parameters to substitutre the position values from this equation.

2.1.3 Solving the Lagrangian of Coupled Oscillator System

The Lagrangian of this system is the following, where the potential energy is the mechanical energy of the springs, and the kinetic energy is the motion of both oscillators

$$L = \frac{1}{2}\left(m_1 \frac{\partial x_1}{\partial t}^2 + m_2 \frac{\partial x_2}{\partial t}^2 - k_1 x_1^2 - k_2 x_2^2 - k_3(x_1 - x_2)^2\right) \tag{16}$$

The equations of motion are as follows,

$$x_1(k_1 + k_3) - k_3 x_2 = m_1 \frac{\partial^2 x_1}{\partial t^2} \tag{17}$$

$$x_2(k_2 + k_3) - k_3 x_1 = m_2 \frac{\partial^2 x_2}{\partial t^2} \tag{18}$$

These equations can be solved by considering the system's oscillation at its eigen-frequency. In this state, the masses harmonically oscillate with the same frequency, either totally in phase, or with a $\frac{\pi}{2}$ phase shift (add citation). Each mass oscillates with some shared frequency, ω, with individual amplitudes a_n. Substituting this standard oscillator solution, $a_n \cos \omega t$, where $\omega = \sqrt{\frac{k}{m}}$,

$$a_1(k_3 + k_1 - m_1\omega^2) - a_2 k_3 = 0 \tag{19}$$

$$a_2(k_3 + k_2 - m_2\omega^2) - a_1 k_3 = 0 \tag{20}$$

These solutions can be expressed as a $2x2$ homogeneous matrix, whos columns are a_1 and a_2,

$$\begin{bmatrix} k_3 + k_1 - m_1\omega^2 & -k_3 \\ -k_3 & k_3 + k_2 - m_2\omega^2 \end{bmatrix}$$

Solving the determinant of this equation yields an expression for ω, or the

The equations of motion of the states of the individual oscillators can be used to solve for the shared frequency, ω, in the case where the determinant of this matrix equals zero. The solution to this case,

$$\omega = \pm\frac{1}{\sqrt{2}}\sqrt{\frac{k_1+k_3}{m_1}+\frac{k_2+k_3}{m_2} \pm \sqrt{\frac{((k_2+k_3)m_1+(k_1+k_3)m_2)^2}{m_1^2m_2^2} - \frac{4(k_2k_3+k_1k_2+k_1k_3)}{m_1m_2}}} \tag{21}$$

We can see this expression is more dynamic than that of an isolated oscillator, or of a single oscillator composed of multiple springs. Equation 11 is composed of the sum of two isolated oscillator factors corresponding to the oscillations of m_1 and m_2, summed with a more complicated, coupling factor under the second square root. For simplicity, we will express this coupling factor as Ω_c^2, and the individual oscillatiing factors as ω_i^2

$$\Omega_c^2 = \sqrt{\frac{((k_2+k_3)m_1+(k_1+k_3)m_2)^2}{m_1^2m_2^2} - \frac{4(k_2k_3+k_1k_2+k_1k_3)}{m_1m_2}} \tag{22}$$

$$\omega_1^2 = \frac{k_1+k_3}{m_1} \tag{23}$$

$$\omega_2^2 = \frac{k_2+k_3}{m_2} \tag{24}$$

such that equation 21 becomes

$$\omega = \pm\frac{1}{\sqrt{2}}\sqrt{\omega_1^2+\omega_2^2 \pm \Omega_c^2} \tag{25}$$

The value ω can be substituted back into either of our solutions of equations 19 and 20 to produce a ratio of the amplitudes of our oscillators in terms of exclusively the parameters of the original equation.

$$a_{12} = \frac{a_1}{a_2} = \frac{m_2}{2k_3}\left(\omega_2^2-\omega_1^2-\Omega_c^2\right) \tag{26}$$

$$a_{21} = \frac{a_2}{a_1} = \frac{m_1}{2k_3}\left(\omega_1^2-\omega_2^2-\Omega_c^2\right) \tag{27}$$

Again, we can see our expression separated into two single frequency factors, and one coupled frequency factor.

2.1.4 Applying Solution to the Coatings Case

Applying the solutions to the equations of motion into equation 28, produces the following expression for the loss angle in terms of the experiment's parameters

$$\phi_2 = \frac{1}{Q_{system}}\left(1+\frac{a_{12}^2k_1}{k_2+k_3(a_{12}-1)^2}\right) - \frac{1}{Q_1}\frac{a_{12}^2k_1+k_3(a_{12}-1)^2}{k_2+k_3(a_{12}-1)^2} \tag{28}$$

Which, by substituting our term for the ratio of the amplitudes, 27, produces an expression for the loss angle in terms of the experiment's parameters

2.1.5 Propagating Error

With coating loss angle as a function of experimental parameters and an observable, its is possible to propagate uncertainties of these measurements into uncertainty of our desiredmeasurement.

By summing in quadrature the propagated uncertainty values, σ, for each parameter α, we retrieve an equation for the total measurement error.

$$\sigma_{\phi_2}^2 = \sum_i \left(\sigma_i \frac{\partial \phi_2}{\partial \alpha_i}\right)^2 \tag{29}$$

The systematic uncertainty of our measurement of the loss angle becomes

$$\begin{aligned}\sigma_{\phi_2}^2 = &\left(\sigma_{k_1}\frac{\partial\phi_2}{\partial k_1}\right)^2 + \left(\sigma_{k_2}\frac{\partial\phi_2}{\partial k_2}\right)^2 + \left(\sigma_{k_3}\frac{\partial\phi_2}{\partial k_3}\right)^2 + \left(\sigma_{m_1}\frac{\partial\phi_2}{\partial m_1}\right)^2 \\ &+ \left(\sigma_{m_2}\frac{\partial\phi_2}{\partial m_2}\right)^2 + \left(\sigma_{Q_1}\frac{\partial\phi_2}{\partial Q_1}\right)^2 + \left(\sigma_{\phi_{system}}\frac{\partial\phi_2}{\partial \phi_{system}}\right)^2\end{aligned} \tag{30}$$

This error model can be displayed as a pie chart in Mathematica to show the relative contribution of the uncertainty of each parameter in the resulting error of the loss angle measurement. Below is a contrived example to show the capability of the Mathematica sliders, and functionality of the pie chart. Following is a figure of the pie chart when more typical values for the experiment are shown.

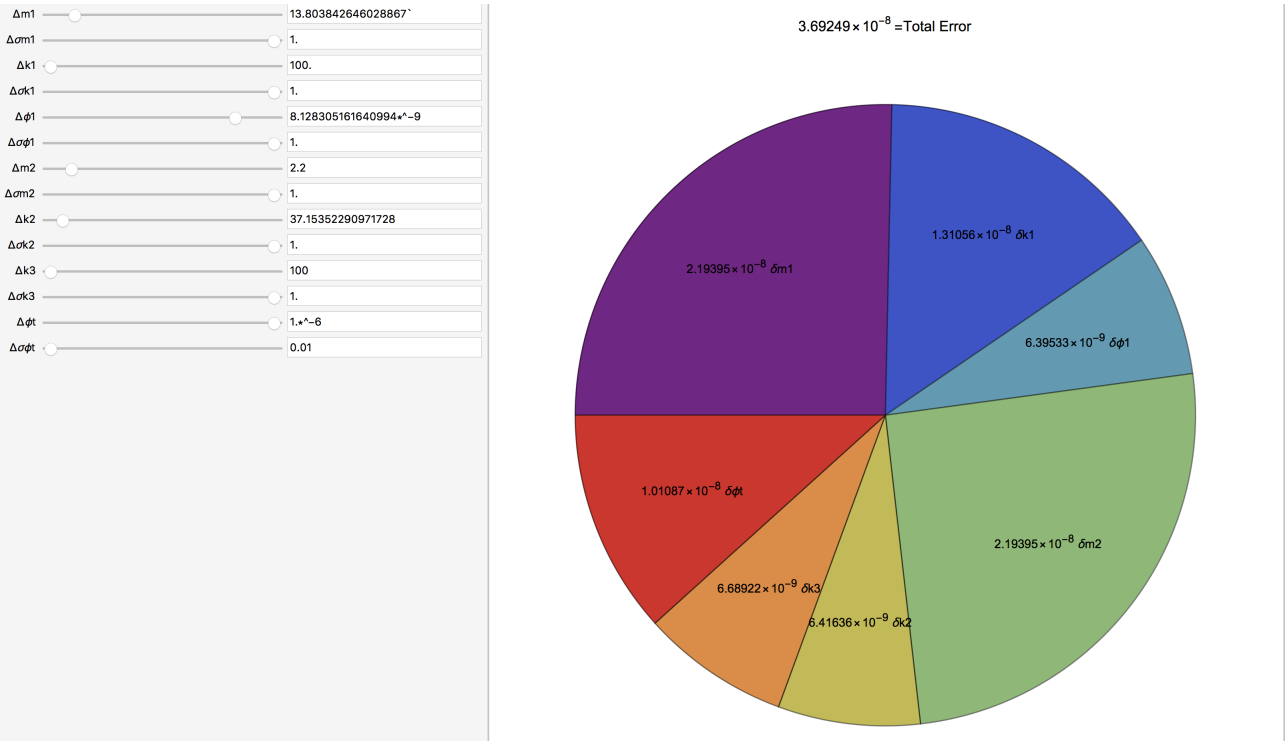

Figure 7: A pie chart of contrived variable values to display its capability. Each piece of the pie is the relative contribution of that parameter to the propagated error. Above the pie chart is the summed uncertainty

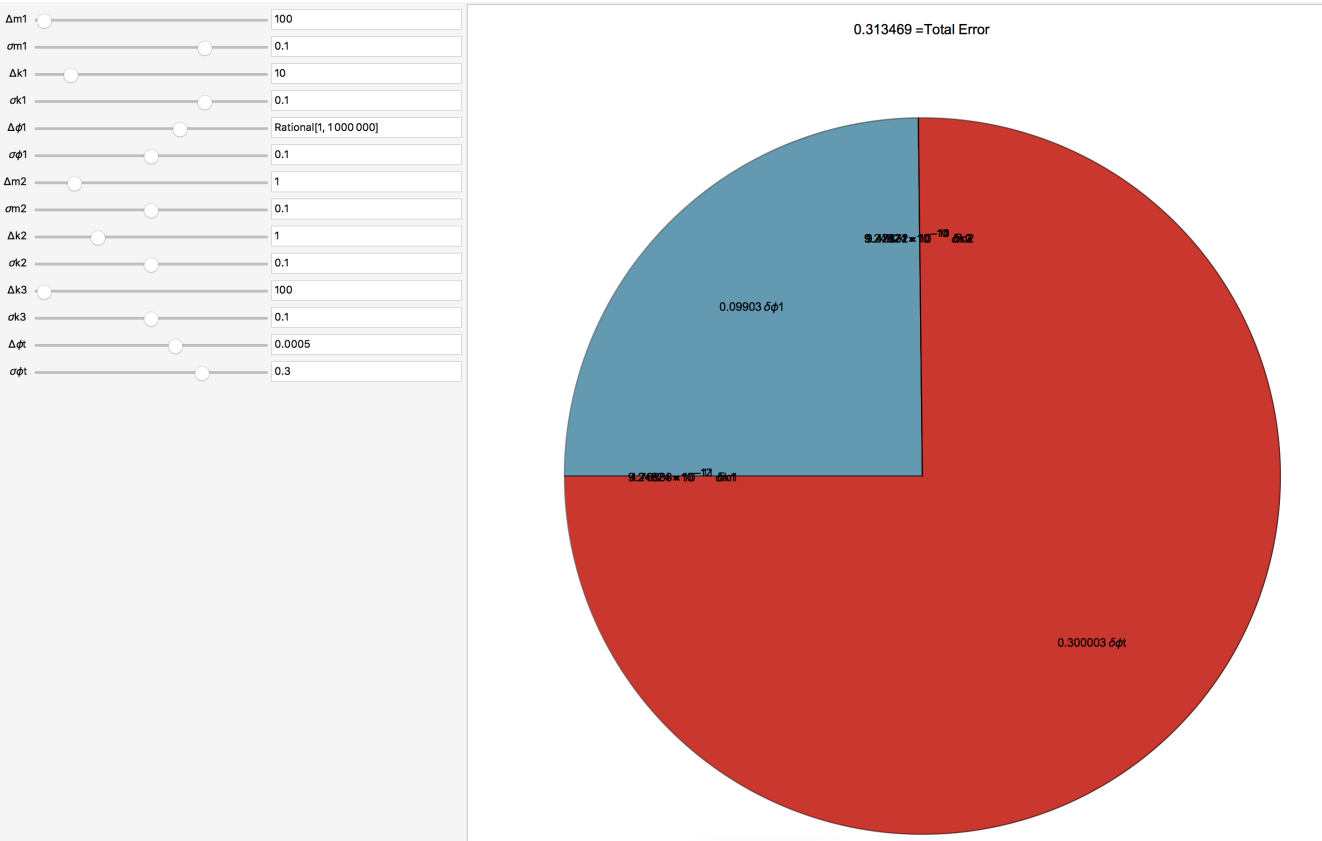

Figure 8: This pie chart displays relative error contributions with parameters more typical of a cryogenic ringdown experiment. The mass of the disk is orders of magnitude larger than the coating, with a much higher spring constant. There is strong coupling between the disk and coatings, and the quality factor of the disk is orders of magnitude higher isolated than with coatings deposited. All uncertainties are defaulted to 10%, with the exception of, the coupled ringdown, placed at 30% at the discretion of Voyager researchers

The error contribution of both the measured coupled loss angle, as well as the loss angle value for the disk contribute a majority of the totaly error of the system by roughly ten orders of magnitude. This is not to say that they are massive contributors of error, rather that parameters of the system that are not loss angle measurement, simply propagate too weakly to significantly affect the end calculation. This model lends valuable information for when more accurate simulations are this coupled system will be run.

2.2 Temperature Tracking of Silicon Eigenmodes

For identifying the temperature dependence of the silicon eigenfrequencies, a modified version of the GeNS is utilized.

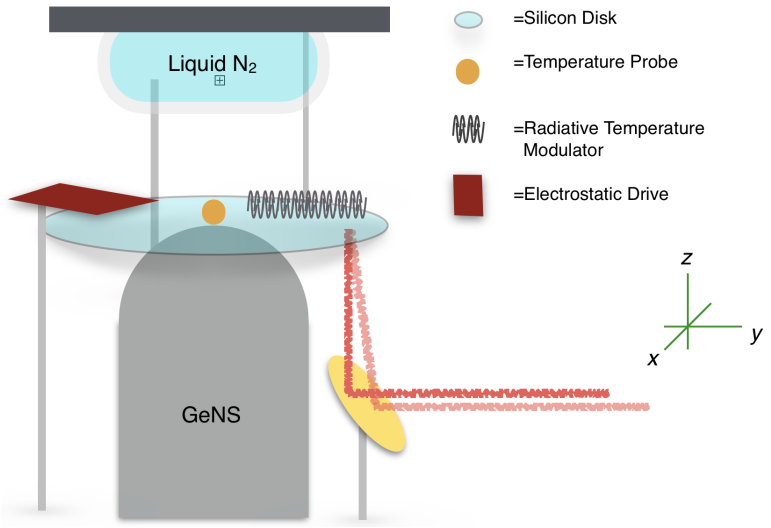

Figure 9: This modified GeNS features both a temperature modulating resistor radiative heater. A temperature probe is thermally contacted to the center of the disk using vacuum rated apoxy. This setup allows the eigenfrequencies to be monitored in frequency space as temperature is decreseased from room temperature to cryogenic temperatures.

The temperature is monitored using a resister temperature detector (RTD) placed on the center of the disk. While this introduced lossy mechanical coupling, the higher order mechanical modes of the silicon disk feature excitations around the fringes of the diskm so this placement should not disturb vibrations by an appreciable amount. Additionally, introducing loss to the system is acceptable in this case because this is a measurement of the location of eigenfrequencies in frequency space, and not that of Q.

2.2.1 Calibrating RTDs

Utilizing in RTD in a Wheatstone bridge configuration allows for precise differential temperature readings. This will be useful for establishing a precise relationship between the temperature and eigenfrequency location of the disk. Additionally, we are utilizing a four lead detection method to reduce lead resistance in the connecting wires, allowing for a more accurate measurement.

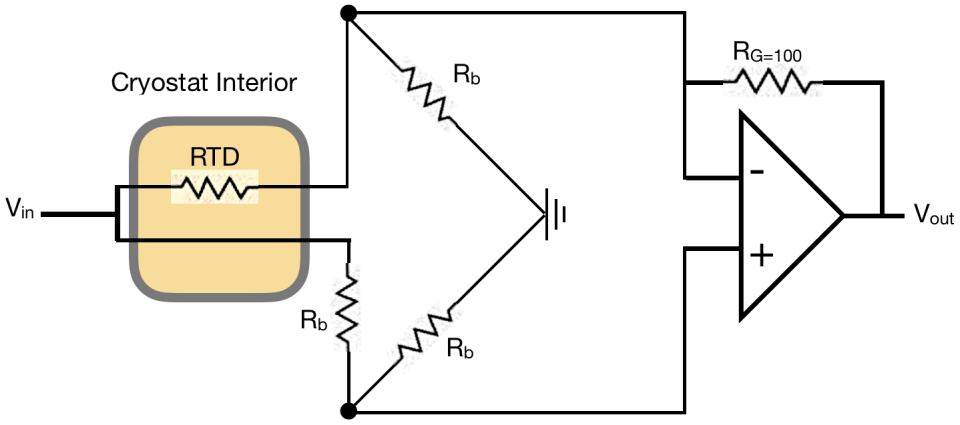

Figure 10: A circuit diagram of the Wheatstone bridge, RTD setup, where $R_{RTD} \approx R_b$. Both leads of the bridge are run through the cryostat, and therefore are the same length and are exposed to the same temperatures, thus factoring lead resistance out of the differential reading.

The voltage is measured across the terminals of the resistor, and are passed through an invertain amplifier with gain G=100. This RTD was calibrated between room and cryogenic temperatures with an applied current of $100\mu A$. The produced voltage - resitance conversion equation of

$$T = V * 14290\frac{K}{V} - 442.9K \pm 4.285K \tag{31}$$

2.2.2 Interior and Exterior Setup

A coiled nichrome wire is used for the temperature modulator, and 100V electrostatic drive is selected for exciting the disk.

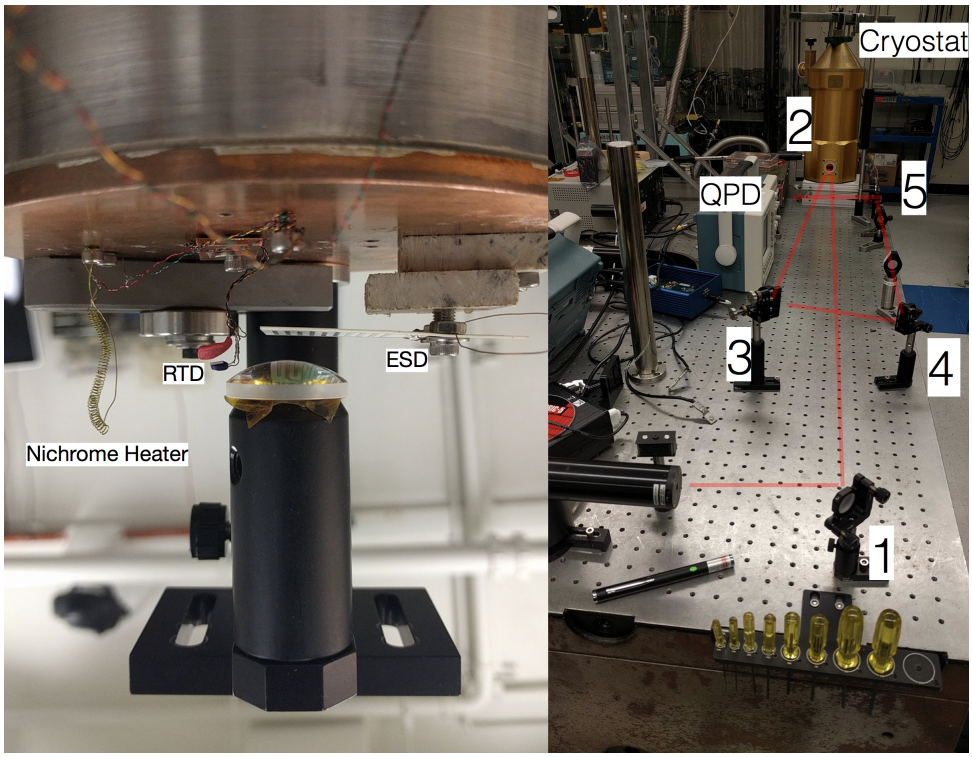

Figure 11: The left figure, the interior setup, shows the relative spacing of the different components. In the final design, the nichrome wire was hung horizontally above the GeNS mount. The right figure, the exterior setup, shows the optical lever path. a HeNe laser is reflected off a mirror (1) into the cryostat (2), where it is incident upon the suspended disk, and reflected into a set of external optics (3). The laser is refocused (4), and reflected into the quadrant photodiode (obscured by an oscilloscope (5)

With this setup complete, the testing of this apparatus could begin. Testing involves calibrating the temperature regulation between the liquid nitrogen tank within the cryostat, and the temperature modulating nichrome wire. The SURF period had expired before testing of this apparatus could begin.

2.3 Thermal Conductance of Copper Straps

2.3.1 Experimental Setup and Diode Calibration

To determine the thermal conductance of the copper straps, the one end of the copper is submerged in liquid nitrogen, while some known quantity of power is applied to the other end. The equilibrium temperature gradient across the strap is measured, and is inserted as the ΔT value in equation **??**. The applied power, provided using a heating resistor, is input as P. The experiment is run in atmosphere, so the strap and resistor are encased in thermally insulating styrofoam. This insulation, though, is not thermally isolating, so the heating from the room temperature environment must be accounted for in equation **??**.

$$k = \frac{P(1 + \frac{\Delta T_{ambient}}{\Delta T_{Resistor}})}{\Delta T_{ambient} + \Delta T_{Resistor}} \tag{32}$$

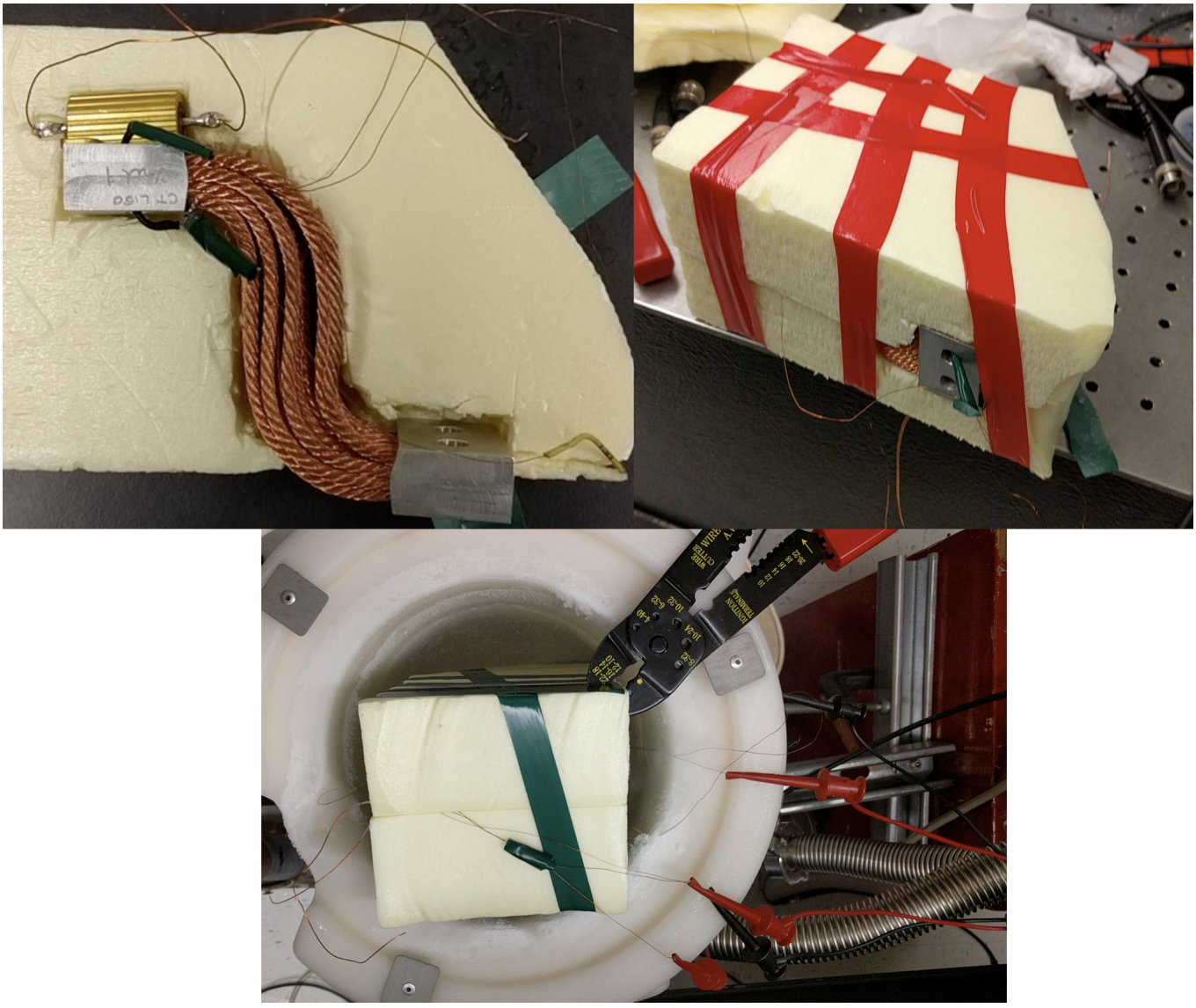

Figure 12: Clockwise from the top left: A picture of the experimental setup. The yellow colored heating resistor is in thermal contact with the top of the strap. Temperature sesors are also in thermal contact with the straps on both ends. In the second picture, the strap is encased in the styrofoam, wrapped tightly in tape. One end of the strap is exposed such that it can be dipped in liquid nitrogen. The last photo demonstrates the tip of the strap immersed in a tub of liquid nitrogen, with wires monitoring the temperature, and supplying current to the resistor connected.

Temperature sensing diodes are used for measuring temperature. Similar to RTDs, these exhibit a linear voltage response to temperature change. The diodes are biased with a $10\mu A$ current.

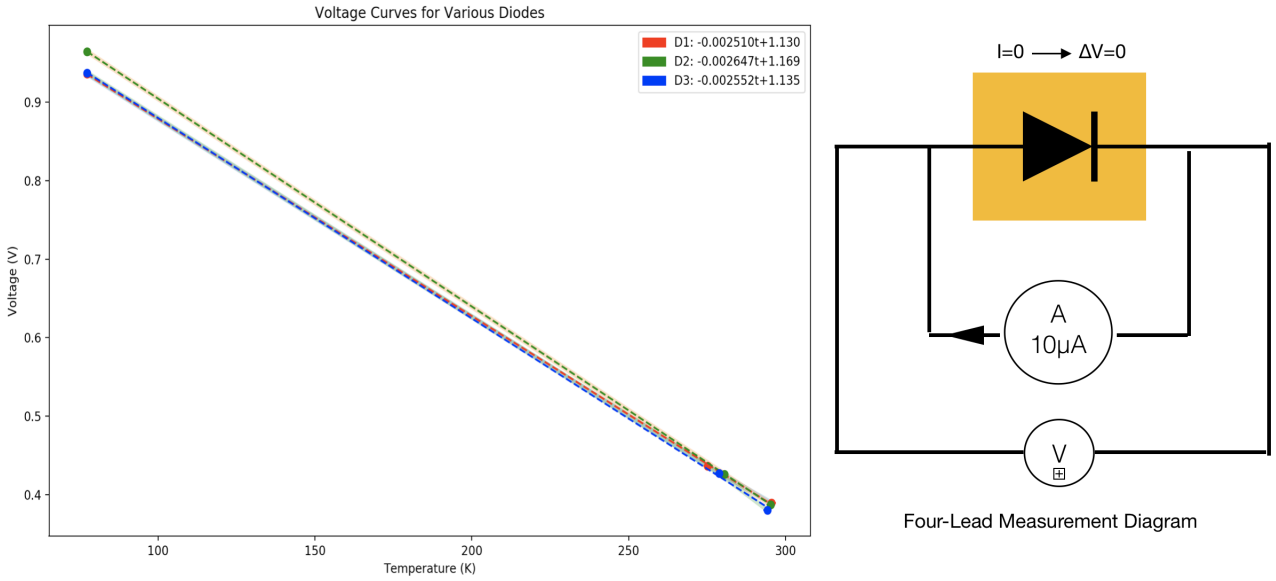

Figure 13: Left: Calibration curve for three separate diodes with the associative linear temperature-voltage equations. Right: A diagram displaying the four-lead measurement technique utilized for biasing and reading the voltage of the diode. Utilizing this method allows the voltage to be read in the absense of a current, eliminating lead resistance.

2.3.2 Experimental Results

After being sealed in the styrofoam, the exposed end of each of the copper straps werre submerged in a tub of liquid nitrogen. Once the temperature across the strap equilibrated, $2W$ of power were injected into the unsubmerged end of the strap. As the liquid nitrogen boiled off, the copper straps were slowly lowered into the tank as to maintain a consistent level of liquid nitrogen exposure. Each trial was concluded after the strap reached thermal equilibrium. Below, the plots for the F and L strap are shown.

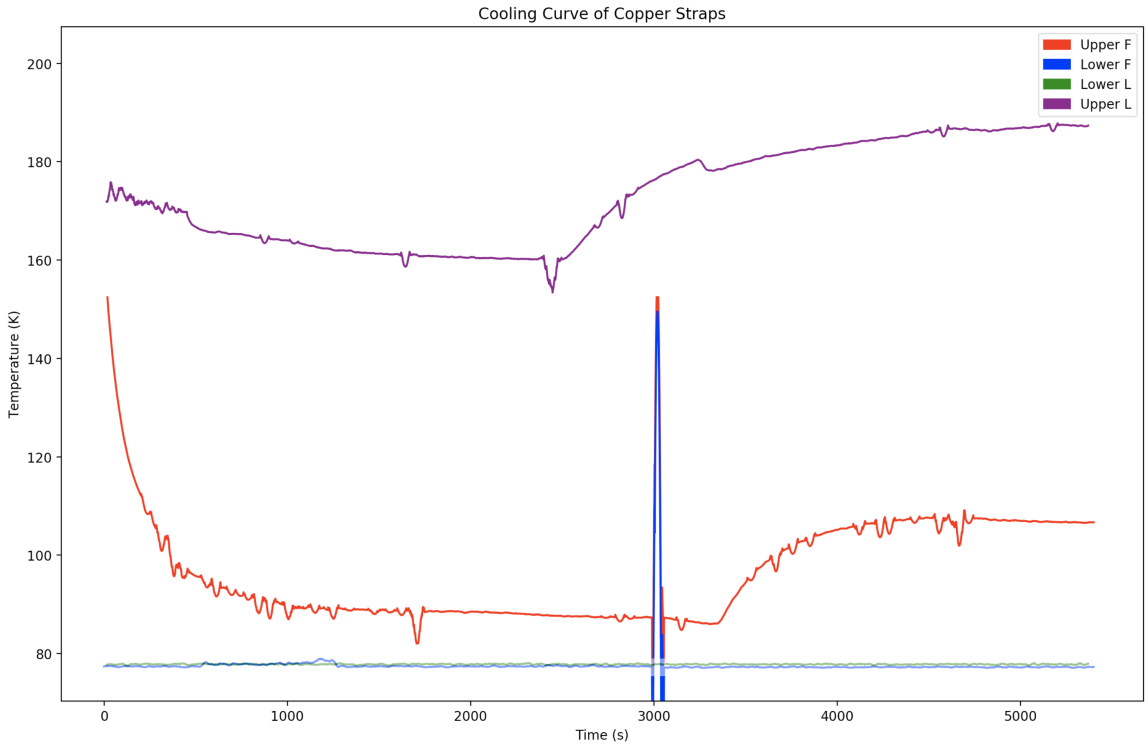

Figure 14: A plot comparing the heating curves of the L and F straps. Upper denotes the temperature of the end of the strap not submerged, while lower is the end of the strap that is not submerged. The feature at t=3000s, is noise from the electronic data acquisition system.

Experimental Results				
Strap Type	Unheated Gradient (K)	Heated Gradient (K)	Power Applied (W)	Conductance (W/K)
S	79.446	106.559	2.013	.01889±.0009
L	82.006	108.673	1.984	.01826±.0009
F	10.062	29.52	1.984	.06721±.0009

3 Discussion

3.1 Coatings Mechanical Loss: Coupled Harmonic Oscillator Modelling

Performing this simple analysis showed that the primary contributions to error in the coatings loss calculation are measurements of the loss of the disk, and the coupled loss of the disk and coating. This will lend insight and intuition for when more detailed finite elementmodels are created, and is even useful for making design decisions in current coatings measurement experiments. It will be interesting to explore whether using more precise parameters such as Young's Modulus will significantly change the orders of magnitude difference between the error contribution between the measured loss angles and other parameters.

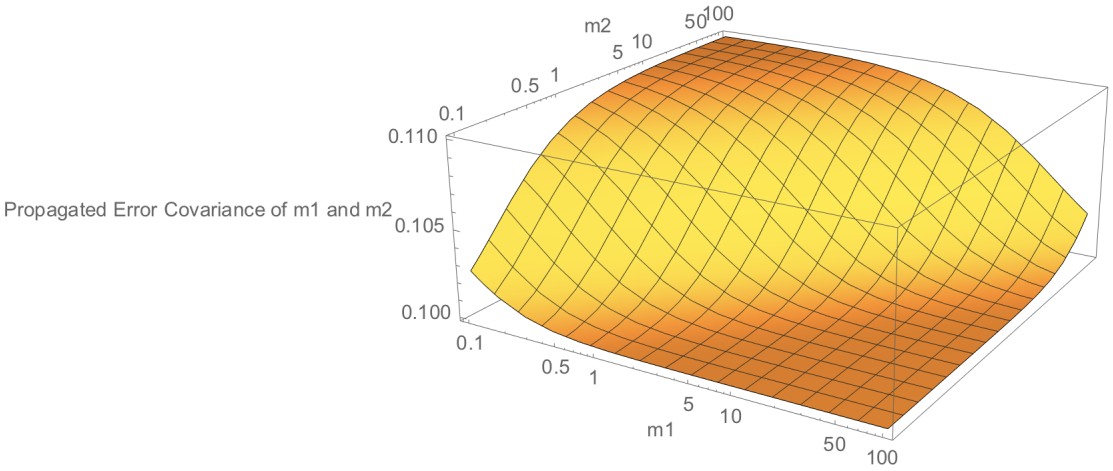

Figure 15: This model can also be used to display the coupling between different parameters of the system. This image shows a plot of the covariance between the two mass parameters. This tool can be used to expose local minima and maxima in parameter space.

The Mathematica code developed for this analysis could be used as a general template for analyzing loss of different coupled systems. Although this instance utilizes an analytical solution, the analysis method is dynamic such that that it can be performed on fits to finite element analysis data, expanding its use. Additionally, I have not found that this sort of analysis has been preformed for the coupled harmonic oscillator before, despite the system being such a common tool for teaching introductory physics. Therefore, in addition to being useful for understanding coupled loss, it could be used as an instructional tool for learning about coupled oscillator systems.

3.2 Temeprature Tracking of Silicon Eigenfrequencies

Due to technical difficulties in the lab, this experiment was unable to progress as expected. Nonetheless, the proper infrastructure is now in place to calibrate the temperature dependence of the silicon disk eigenfrequencies as a precursor for coatings analysis. This will prove very useful for performing future coatings analysis using the GeNS, as now the temperature of the disks can be monitored without mechanically coupling the disk to a lossy thermal probe.

3.3 Thermal Conductance of Copper Straps

It is evident that the F strap is a better thermal conductor. This is at no surprise for multiple reasons. The F strap is a lot more dense of a strap than the equivalently dense S and F straps, as suggested by the higher cross sectional area. This translate to a much higher cooling power as there are more thermal conduction paths available between the ends of the strap. The F strap is also much shorter, meaning the temperature gradient is established over a much smaller distance.

Physical Parameters			
Strap Type	Cross Sectional Area (mm^2)	Length (m)	Conductivity (W/mK)
S	68.3	200	284.76±10
L	68.3	214-200	260.60±10
F	319.2	100	34.88±5

In a measurement that factors in geometry, such as thermal conductivity (this is a measurement of conductance), the dimensional parameters of cross sectional area and length would be factored into the final value, providing a measurement of the material used in the straps. In the above table, this calculation is performed. The conductivity of the S and L straps is evidently much higher than the F strap, suggesting the conductive material used is of much higher quality. Nonetheless, this experiment had the purpose of which strap, regardless of geometry, was a stronger conductor, and that was shown to be the F strap.

With the conductance of the straps determined, it is now important to determine the mechanical properties.In a similar manner to the GeNS, a spectral analysis can be performed on reflected laser incident upon the straps under use. This will be useful in identifying which frequency bands the straps are excited at. The use of accelerometers can be employed as well to measure the mechanical transfer function of the straps. These values, in conjunction with the thermal properties determined in this paper, will help Voyager determine which copper strap is most suitable for implementation in LIGO Voyager. This form of analysis can be performed with the use of a vibrometer.

References

[1] Abernathy M R, *et. al.*, *Measuerment of mechanical loss in the Acktar Black coating of silicon wafers.* IOP Publishing, Classical and Quantum Gravity, **33**, 185002 (2016).

[2] Adhikari R, *et. al.* , *LIGO Voyager Upgrade Conceptual Design.* Laser Interferometer Gravitational Wave Observatory (2013).

[3] Cesarini E, *et. al.*, *A "gentle" nodal suspension for measurements of the acoustic attenuation in materials.* Review of Scientific Instruments, **80**, 053904 (2009).

[4] Schnabel R, *et. al.*, *Building blocks for future detectors: Silicon test masses and 1550nm laser light.*

[5] Vajente G, Gustafson E, Adhikari R, *Amorphous Coatings Development Program.* G1601305 -v11.

Consulted with Professor Rana Adhikari, Dr. Brittany Kamai, and Aaron Markowitz. Revisions and suggestions provided by Dr. Kamai and Aaron Markowitz